PERGAMON

International Journal of Multiphase Flow 25 (1999) 349–364

International Journal of Multiphase Flow

Cavity outflow from a nearly horizontal pipe

W.H. Hager *

VAW, ETH-Zentrum, CH-8092 Zurich, Switzerland

Received 17 September 1997; received in revised form 13 July 1998

Abstract

Outflow from a circular pipe is considered for cavity flow. The cavity geometry, the end depth and the jet trajectories are described, in terms of the pipe Froude number. This is an extension of previous work for pipes sufficiently large such that effects of viscosity and surface tension can be neglected. © 1999 Elsevier Science Ltd. All rights reserved.

Keywords: Benjamin bubble; Cavity flow; Jet trajectories; Long bubble; Pipe

1. Introduction

Outflow from a pipe that is nearly horizontal exhibits a peculiar transition between free surface and pressurized flow conditions. The so-called cavity outflow consists of an upstream pressurized and a downstream free surface flow portion. For pipes sufficiently large, the effects of viscosity and surface tension can approximately be neglected, and a purely gravitational flow may be considered, in which effects of streamline curvature are significant. The previous findings of Cola and Benjamin are generalized by accounting for the flow configuration close to the efflux section.

Cavity outflow from pipes is relevant in various domains, including the emptying of long-necked bottles, applications in hydraulic engineering and industrial hydraulics. There is a particular relevance in the range of occurrences, and it is demonstrated that the pipe slope has a relatively small effect on the outflow features. Expressions are derived for the cavity shape, the end depth ratio and the nappe geometry. The results depend mainly on the pipe Froude number f and a generalized approach is given for the circular pipe. All results are readily applicable for design purposes, and a distinction between cavity outflow and bubble washout is

* Corresponding author.

0301-9322/99/$ - see front matter © 1999 Elsevier Science Ltd. All rights reserved.
PII: S0301-9322(98)00046-9

made. The computations are demonstrated to be in essential agreement with laboratory observations.

2. Review

Cola (1965) considered a semi-infinitely long horizontal duct of rectangular cross-section *initially* filled with water. If the barrier is abruptly removed, a water wave similar to a dambreak wave is set up, with a negative wave propagating into the upstream reach and emptying this portion, and a positive wave propagating into the initially dry duct portion. The emptying process can be approximated with the Ritter solution for the dambreak wave (Liggett, 1994):

- positive front velocity is $+2(gd)^{1/2}$;
- negative front velocity is $-(gd)^{1/2}$;
- flow depth at rupture section is $(4/9)d$; and
- discharge at rupture section is $(8/27)(gd^3)^{1/2}$.

These relations hold as long as the negative front has not reached the upstream end of the duct.

Cola was able to demonstrate that point S of the negative front location deserves particular attention. Because the energy head is initially equal to its height d, and assuming a velocity equal to the propagation velocity $-(gd)^{1/2}$, one would have $H_A = d + (gd)/(2g) = (3/2)d$. This result is demonstrated to be in error, mainly because of streamline curvature effects. In fact, point S corresponds to a stagnation point for an observer moving with the propagation speed $c = -(gd)^{1/2}$, and Cola demonstrated that the upstream pressure head curve is located by $-c^2/(2g)$ below the vertex of the duct. For an observer moving with a velocity c, the stagnation point remains thus steady and the velocity head is compensated for by the depression height, such that the energy head is $H = h_c = d$ along the entire duct, provided friction is neglected.

From energy considerations, it can be demonstrated that flows with $Y > 0.5$ are physically impossible. Cola (1965) introduced two cases of flow (Fig. 1):

1. $Y = 0.50$ as a potential flow with a smooth reduction of flow depth from the stagnation point to the asymptotic downstream depth; and
2. $Y < 0.5$ as a flow with a finite energy dissipation, due to the formation of a hydraulic jump.

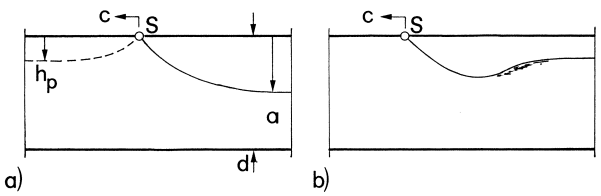

Fig. 1. Bubble propagating in rectangular duct: (a) potential flow; (b) dissipative flow (Cola, 1965).

Cola (1967) extended his study to circular pipes of diameter D. Observations indicate substantial agreement with predictions regarding propagation velocity, and upstream subpressure head. For potential flow, the downstream pipe filling obtains $a/D = 0.681$, thus considerably larger than for the rectangular duct.

Benjamin (1968) is currently considered as the first having introduced the phenomenon, and it seems that the contributions of Cola are not sufficiently acknowledged. The particularity of Benjamin's paper is its reference to a much larger field of applications than the hydraulic studies of Cola, with the results being basically identical. For the circular pipe, Benjamin found an asymptotic downstream depth $a/D = 0.580$ instead of 0.681, and experiments to be discussed below indicate approximately $a/D = 0.630$. Whereas Cola determined the free surface profile graphically, Benjamin used conformal mapping. For a rectangular duct, the angle at the stagnation point is 30°.

Cola (1970) considered outflow from a horizontal pipe by introducing the so-called pipe Froude number $f = V/(gD)^{1/2}$, with V as the pipe full-flow velocity. Free surface flow occurs for $f < 0.62$ and the pipe is fully pressurized for $f > 1.10$. The effect of downstream submergence on the pipe outflow was also investigated.

Wallis et al. (1977) considered the outflow from a horizontal pipe using a basic hydraulic approach. They distinguished: (1) critical flow for partial pipe filling; (2) bubble flow; (3) bubble washout; and (4) full pipe flow. It was demonstrated that both viscosity and surface tension effects are negligible provided the pipe diameter is larger than 100 mm, and the fluids involved are water and air. Comparable results followed also from Wilkinson (1982).

The contributions of Bendiksen (1984), and Alves et al. (1993), among others, refer to the drift velocity in a pipe where a large bubble advances. Baines et al. (1985) investigated the effect of downstream submergence on the bubble flow pattern, and Couët and Strumolo (1987) analyzed the effect of surface tension on bubbles rising in an arbitrarily sloping tube. Also, they presented solutions for the bubble geometry in a potential flow, by including surface tension.

Montes (1997) studied the configuration also treated below. Incipient cavity flow was identified for $f = 0.51$, and incipient pressurized flow for $f = 1.06$, subject to some variation when compared with other results. The cavity is computed for a potential flow configuration.

3. Experiments

The internal pipe diameter was $D = 240$ mm to inhibit scale effects. According to the literature review, effects of surface tension and viscosity are thus negligible. The plexiglass pipe had a length of 16 diameters and was connected to the supply pipe. The set-up was mounted in an existing rectangular channel 0.50 m wide and the instrumentation was available. Free surface depths downstream of the stagnation point were measured by the circumference, form the pipe vertex to the free surface by accounting for the pipe thickness of 8 mm. Previous experiments indicated maximum deviations of about ± 2.5 mm. Velocities at the end section of the pipe were measured with a conventional propeller meter of internal diameter 8 mm. The transverse variation of velocity at the end section was small, and only the axial velocity distribution was measured. The nappe profiles downstream from the pipe were observed with

point gages to the nearest millimeter. For the lower nappe of the outflow jet, an inverted point gage was used.

The discharge was measured with a triangular V-notch weir to $\pm 2\%$ or $\pm 0.2\,l\,s^{-1}$, whichever was larger. The bottom slope of the pipe was varied as $S_0 = -0.01$, 0, and $+0.01$, and the effect on cavity outflow was extremely small. In a special series of experiments, the transition from the supply to the test pipe was throttled with a plate of 50% opening of half-circular shape. The approach flow to the test pipe involved then a bottom jet which expanded into the test pipe, over a length of about $3D$. Because cavity lengths smaller than $10D$ were studied, there remained a length of about $3D$ for flow development. No effect of the plate on the cavity flow could be detected, and it follows that cavity flow is extremely stable to upstream flow perturbation. For any given bottom slope S_0, a discharge sufficiently large was selected and the top portion of the outflow section was blocked so as to force a hydraulic jump in the pipe. Once the transition from free surface approach to pressurized pipe flow occurred, the approach portion deaerated and the hydraulic jump moved upstream. All air was washed downstream and the pipe started to run fully pressurized without any air bubbles in the flow.

The following results refer to the cavity shape, the end depth ratio for cavity outflow, the location of the stagnation point relative to the end section and velocity distributions at the end section, as functions of the pipe Froude number. Also, the nappe profiles downstream from the end section are discussed.

4. Description of flow

Consider a nearly horizontal and large circular pipe that terminates at the end section. Those pipes may flow either fully pressurized with water, or partially filled with a stratified air-water flow. The transition from partially filled to pressurized pipe flows is complex and involves mixtures of air and water in general. The present problem is particular as mixture flow does not occur, but the transition includes both free surface and pressurized flows. Three cases may be distinguished (Fig. 2):

1. free surface flow, with an asymptotic approach flow depth and a drawdown to the end section, provided the discharge is smaller than the lower transition discharge Q_a;
2. upstream pressurized flow, with a stagnation point S, followed by free surface flow decreasing toward the end section;
3. fully pressurized flow with a discharge larger than the upper transition discharge Q_p, with a circular jet discharging into the atmosphere.

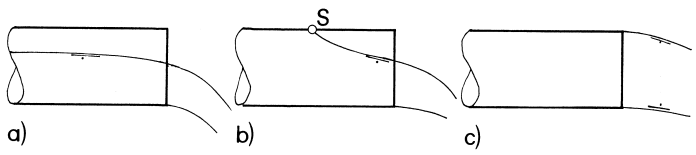

Fig. 2. Types of pipe outflows.

The location of the stagnation point and the outflow jet features depend significantly on the so-called *pipe Froude number* $f = V/(gD)^{1/2}$ where V is the average velocity in the pressurized pipe reach, g the gravitational acceleration and D the pipe diameter. The transition Froude numbers determined in the present study are $f_a = 0.544$ and $f_p \cong 1.15$. For $f < f_a$ the pipe runs partially filled, and fully pressurized flow occurs for $f > f_p$.

Fig. 3 shows outflow geometries of pipe flows for various values of f. For $f = 0.804$ the cavity is nearly washed out of the pipe, with a transition length $X_t = x_t/D = 0.60$ [Fig. 3(a)], where x_t is the distance from the time-averaged stagnation point to the end section. For $f = 0.73$ [Fig. 3(b)] this length is somewhat larger ($X_t = 0.9$) but the outflow is similar to the previous case. For $f = 0.693$ [Fig. 3(d)] the inflexion point of the free surface is almost at the end section and the cavity length is $X_t = 1.1$, i.e. larger than the diameter, and $X_t = 1.8$ for $f = 0.657$ [Fig. 3(d)]. Decreasing the relative discharge by only −3% to $f = 0.639$ makes the cavity length significantly longer to $X_t = 3.0$ [Fig. 3(e)]. This flow has a horizontal reach between the stagnation zone and the drawdown close to the end section. Then, the approach of Benjamin (1968) applies, and cavities shorter than 3 diameters are different from long cavities. One may distinguish between:

- bubble washout for $X_t \leqslant 3$, i.e. $f \geqslant 0.64$; and
- cavity outflow for $X_t > 3$, i.e. $f < 0.64$.

For $f = 0.586$, the cavity length is about 6.8 [Fig. 3(f)], and the horizontal flow portion is considerable. A lower limit value $f = 0.548$ was attained, but experiments were then influenced by the detailed supply geometry. Also, the transition from cavity outflow to free surface flow depended considerably on the bottom slope. The lower limit value is also influenced by the surface roughness of the pipe, given the large values of X_t. Montes quoted values between $f_a = 0.51$ (own experiments) and $f_a = 0.64$ (Smith). For the sake of approximation of the present data, a computational value $f_a = 0.544$ is adopted (Montes, 1997).

Top views on the cavities are shown in Fig. 4. For large f, the bubble fronts have a larger radius of curvature than for smaller f. Also, the bubble front was more stable for large f. Typical profiles for cavity outflow are presented in Fig. 5. The angle of the profile at the stagnation point is 33° (±3°), and the constant depth ratio is 0.625 ± 0.02.

For cavity outflow there is a tendency of wave formation with a wave amplitude of about $\pm 0.02D$. This tendency grows with decreasing f, and the transition to free surface pipe flow is always accompanied with a downstream wave formation. Fig. 6 shows sequences of the transition with the 50% gate mounted at the upstream end of the channel (as previously described). First, the wave breaks [Fig. 6(a)], an air pocket moves upstream to the space downstream of the gate with a low pressure zone [Fig. 6(b)], and the outflow from the supply pipe is aerated [Fig. 6(c)]. The air entrained by the jump is transported downstream into the cavity, associated with a build-up of the subpressure again. The cavity flow develops another breaking wave [Fig. 6(d)], and the next air pocket is transported upstream. For certain values of f, depending on the pipe slope, this cycle could be maintained, and the formation of an isolated slug could be observed. Once the value f was decreased below $f = 0.50$, say, slugs disappeared and a stable free surface flow was established. Here, we refer exclusively to cavity outflow.

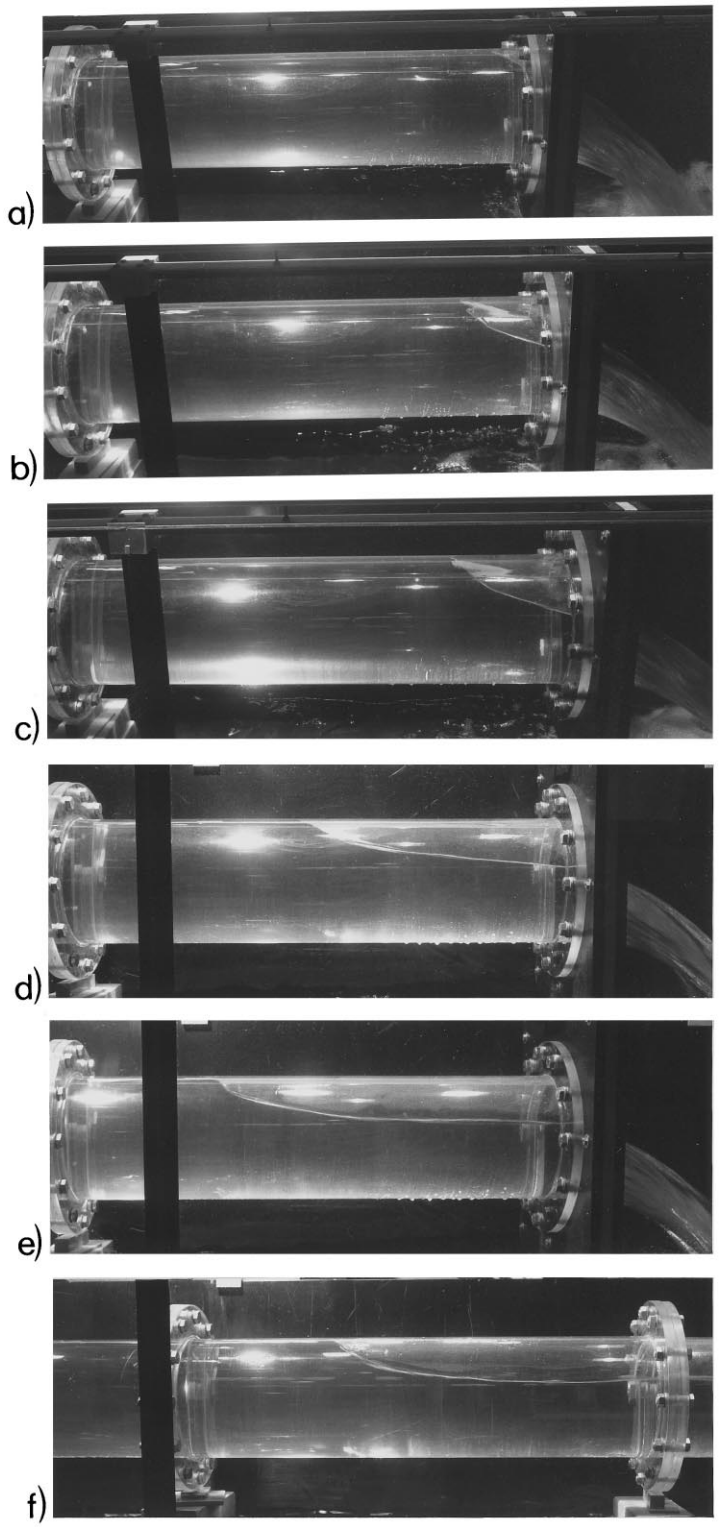

Fig. 3. Bubble shapes for cavity outflow from a circular pipe. f = (a) 0.804; (b) 0.731; (c) 0.693; (d) 0.657; (e) 0.639; (f) 0.586.

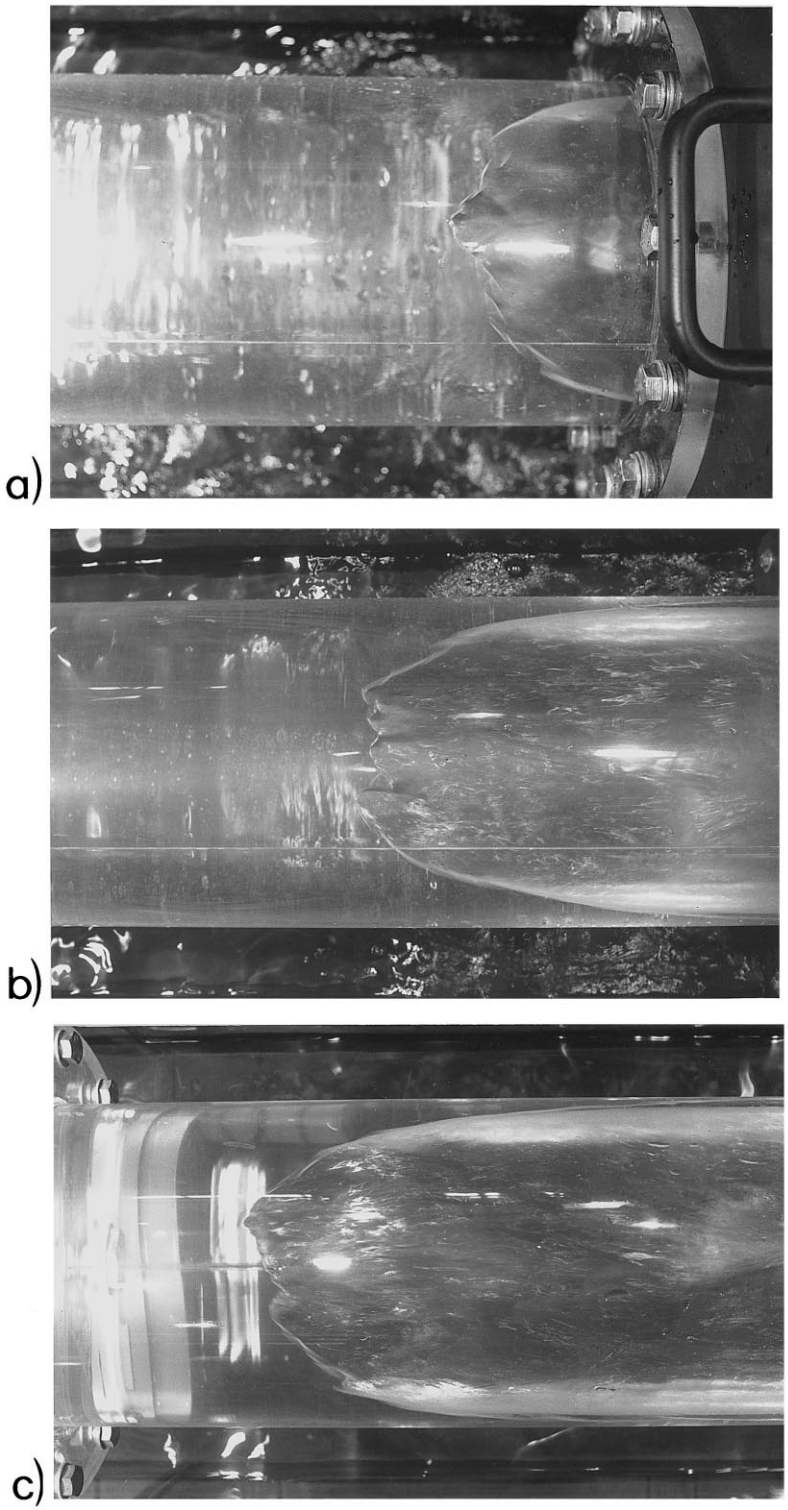

Fig. 4. Top views on bubble nose close to stagnation point. f = (a) 0.731; (b) 0.657; (c) 0.586.

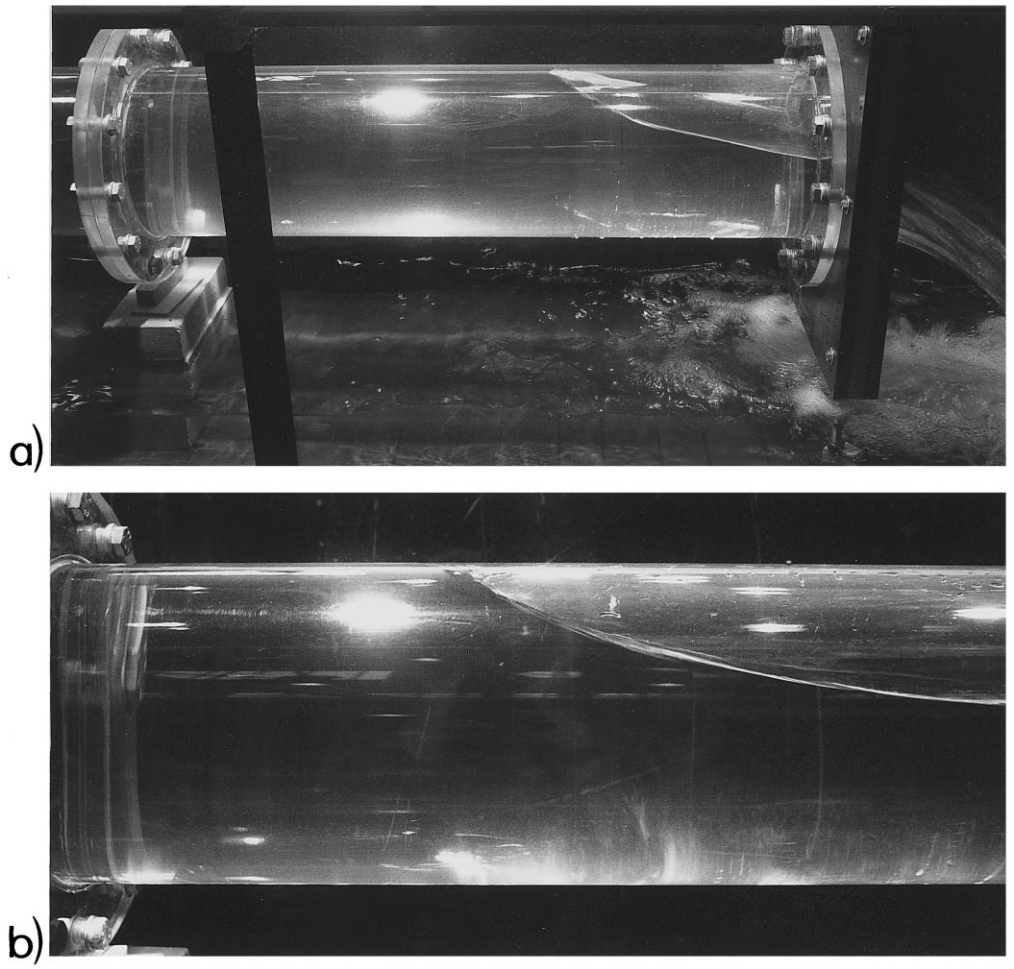

Fig. 5. Side views of cavities for f = (a) 0.657; (b) 0.586.

5. Bubble shape

5.1. Rectangular channel

The shape of a steady Benjamin (or Cola) bubble in a sufficiently large channel involves streamline curvature effects, and the influences of both viscosity and surface tension can be neglected. The governing equation of the free surface profile involves an extended Boussinesq equation derived by Hager and Hutter (1984). For potential flow, the energy head $H = h_0$ remains constant and equal to the duct height in a horizontal channel of rectangular cross-section. With h as the pressure head, q as the discharge per unit width, g as the gravitational acceleration and $h' = \mathrm{d}h/\mathrm{d}x$, $h'' = \mathrm{d}^2h/\mathrm{d}x^2$ as derivatives of the pressure head profile $h(x)$,

$$H = h_0 = h + \frac{q^2}{2gh^2}\left[1 + \frac{2hh'' - h'^2}{3}\right]. \tag{1}$$

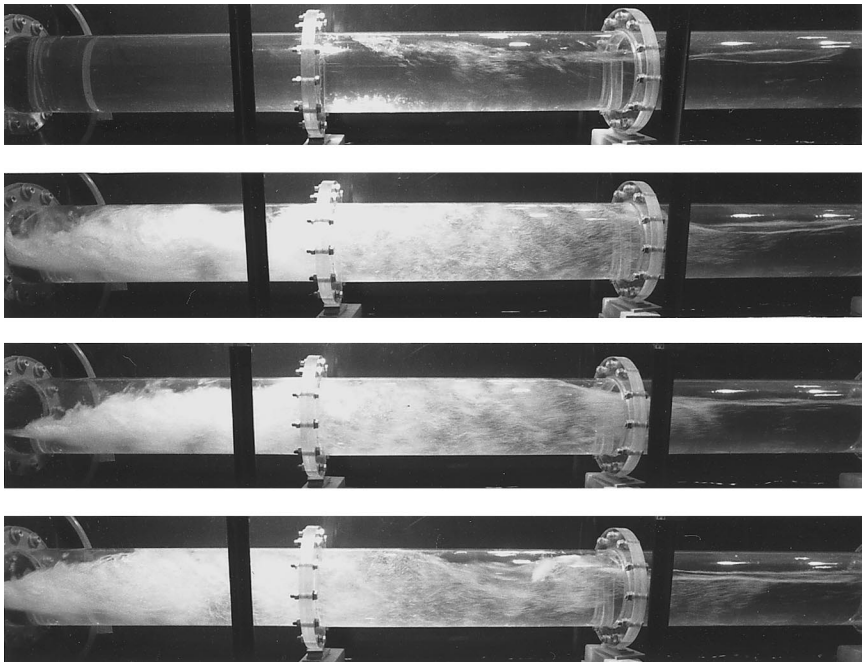

Fig. 6. Transition from cavity to slug flow (details in text).

The derivatives of $h(x)$ drop for the asymptotic downstream depth $h = a = (1/2)h_0$ to yield $q^2/(2ga^3) = 1$, or $F_a = q/(ga^3)^{1/2} = 2^{1/2}$. These results are due to Benjamin (1968).

Introducing dimensionless coordinates $X = x/a$ and $y = h/a$, (1) may be expressed as

$$2 = y + y^{-2}\left[1 + \frac{2yy'' - y'^2}{3}\right]. \tag{2}$$

A first integration subject to the boundary conditions $y'(y = 1) = 0$ and $y(X = 0) = 2$ gives

$$y'^2 = \frac{3}{2}[2 - 5y + 4y^2 - y^3] = \frac{3}{2}(y - 1)^2(2 - y). \tag{3}$$

For $y = 2$ the slope of the pressure head line is $y' = 0$ as required. Integration of (3) gives

$$y = 2 - \tanh^2[(3/8)^{1/2}X]. \tag{4}$$

The profile $y(X)$ is similar to a solitary wave of amplitude $y = 2$, i.e. of double height compared to the asymptotic free stream depth $y = 1$ [Fig. 7(a)].

The free surface profile $T(X)$ where $T = t/a$ is the height of the free surface above the channel bottom can simply be expressed in terms of y as (Hager and Hutter, 1984)

$$\frac{T}{y} = 1 + \frac{1}{2}y'^2, \text{ i.e. from (3),} \tag{5}$$

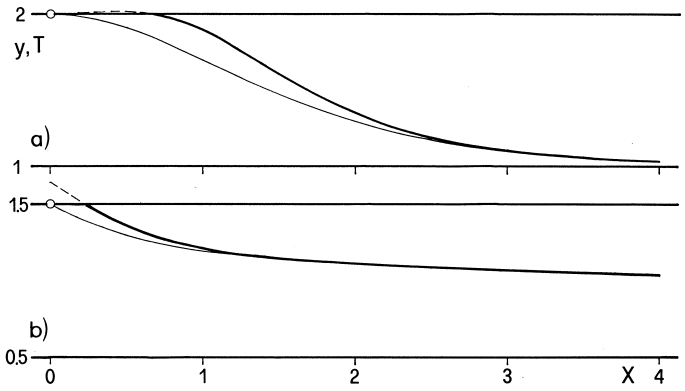

Fig. 7. (—) Pressure head profile $y(X)$ and (—) free surface profile $T(X)$ for (a) rectangular duct and (b) circular pipe.

$$\frac{T}{y} = 1 + \frac{3}{4}(y-1)^2(2-y). \tag{6}$$

The free surface slope $T'(T=2)$, i.e. $T'(y=1.85)$ from (6) is $T'(T=2) = -0.175$ (–9.9°). Further downstream, the free surface slope increases up to the point of inflection $y = 5/3$, where $y'^2 = 2/9$ from (3) and thus $T' = -0.523$ (–27.6°). Close to the DUCT vertex, the free surface slope is almost constant at –0.5, and the bubble shape may be approximated as [Fig. 7(a)]

$$T = 2 - \tanh[(2/3)\bar{X}]. \tag{7}$$

Here, $\bar{X} = X - 0.8$ is the origin of the bubble. Compared to the mathematically exact solution, (7) has a linear decrease of flow depth close to $T = 2$. Because capillary effects are significant close to the vertex, this domain is not properly reproduced with the present approach.

5.2. Circular conduit

The cross-sectional area $F(h)$ of a partially filled conduit is involved, and conduits with a filling ratio larger than $h/D = 0.4$ may be approximated (6%) as a substitute rectangular channel

$$F = (\pi/4)hD. \tag{8}$$

The conduit may thus be considered as a rectangular channel of substitute with $b = (\pi/4)D$.

Benjamin (1968) determined the asymptotic flow depth in a circular conduit to $a = 0.563D$, or $A = 1.776$. The modified (1) can be expressed for the substitute rectangular channel as

$$H = h_0 = D = h + \frac{Q^2}{2gb^2h^2}\left[1 + \frac{2hh'' - h'^2}{3}\right], \tag{9}$$

with $Q/(gD^5)^{1/2} = (\pi/4)A^{-3/2}[2(A-1)]^{1/2}$ where $A = D/a$, $y = h/a$ and $X = x/a$. Note that the maximum discharge is $Q_M/(gD^5)^{1/2} = (\pi/4)(2/3)^{3/2}$ for $A = 3/2$. Inserting in (9) gives

$$A = y + (A-1)y^{-2}\left[1 + \frac{2yy'' - y'^2}{3}\right]. \tag{10}$$

For $A = 2$, (10) reduces to (2). Integrating for the boundary condition $y'^2(y = 1) = 0$ gives

$$y'^2 = \frac{3}{2}\frac{(y-1)^2(2A-2-y)}{(A-1)}. \tag{11}$$

For $A = 3/2$ retained previously, this yields

$$y'^2 = 3(y-1)^3. \tag{12}$$

Integrating a second time subject to the boundary condition $y(X = 0) = (3/2)$ gives [Fig. 7(b)]

$$y = 1 + [2^{1/2} + (3^{1/2}/2)X]^{-2}. \tag{13}$$

Fig. 7 compares the two solutions (4) and (13) and the main difference is at the transition from pressurized to free surface flows. The present model does not account for surface tension. Therefore, the general trend of free surfaces for both rectangular and circular conduits is similar. The latter can be approximated with $\bar{X} = X + 0.25$ as

$$\frac{t}{a} = 1 + 0.5\exp(-\bar{X}). \tag{14}$$

With $T = t/D$ and $\chi = \bar{x}/D$ where $\bar{x}$ is measured from the transition point, (14) may be explicitly expressed as [Fig. 7(b)]

$$T = \frac{2}{3}\left[1 + 0.5\exp\left(-\frac{3}{2}\chi\right)\right]. \tag{15}$$

Experiments are used to verify the prediction.

6. End depth ratio

The end depth ratio $y_e = h_e/D$ with h_e as the end depth [Fig. 8(b)] can be determined with the momentum equation provided the pressure conditions are correctly accounted for. For cavity outflow, the residual pressure at the outflow section is negligible (Hager, 1983). For bubble washout the flow conditions are modified, however, because of velocity and pressure interaction close to the efflux section. These uncertainties are packed into a pressure coefficient, σ, and the modified momentum equation reads, in analogy to Cola (1967) or Benjamin (1968)

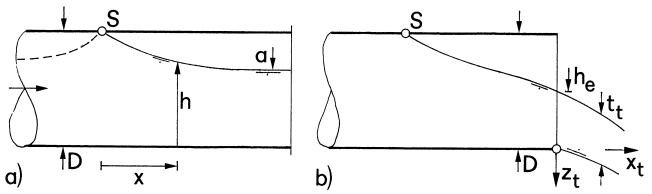

Fig. 8. (a) Cavity flow in an infinitely long circular pipe; (b) cavity outflow close to end section.

$$\frac{\rho Q^2}{(\pi/4)D^2} + \frac{\rho g \pi D^3}{8} - \sigma \frac{\rho V^2}{2} \frac{\pi D^2}{4} = \frac{\rho Q^2}{(\pi/4) D h_e}. \tag{16}$$

Here, the outflow section has been approximated as given in (8). Substituting $f = V/(gD)^{1/2}$ and solving for $y_e = h_e/D$ gives

$$y_e = \frac{2f^2}{1 + f^2(2 - \sigma)}. \tag{17}$$

For $\sigma = 1$ the solution for cavity outflow is obtained. Cola (1967) determined the pressure head $2.4D$ upstream from the end section as $\sigma = 1/2$. However, the pressure at the end section is not contained yet, and $\sigma = 2/3$ can be adopted. Eq. (17) holds for $0.544 < y_e < 1$, i.e. for $0.65 < f < 1.20$.

7. Experimental results

Fig. 9 shows pipe outflow for various values of f. The value $f = 1.16$ corresponds to the upper limit of discharge, with the pipe just fully pressurized, and the jet of initial height D.

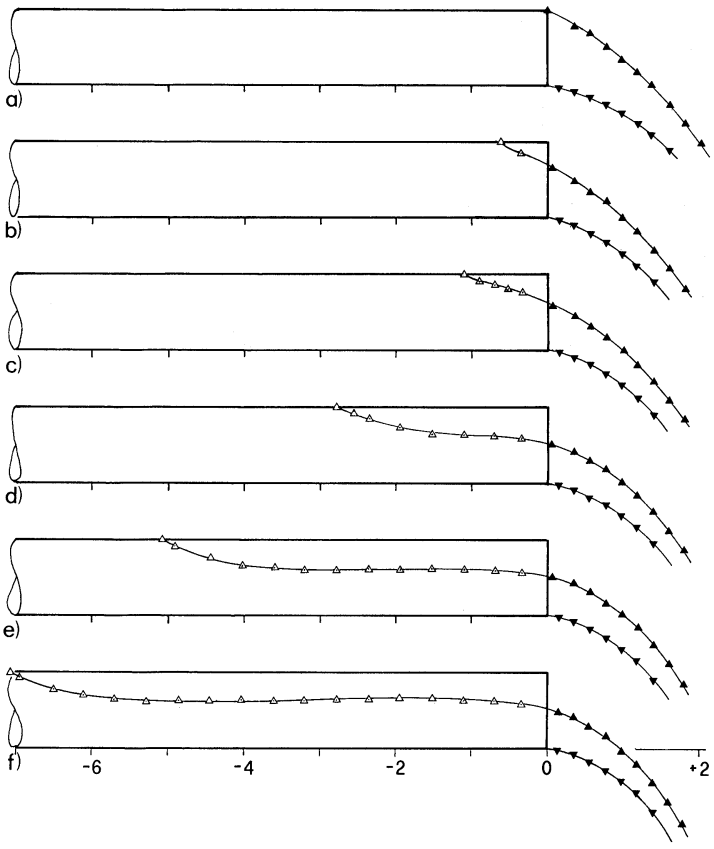

Fig. 9. Cavity and nappe profiles for $f =$ (a) 1.16; (b) 0.794; (c) 0.700; (d) 0.641; (e) 0.628; (f) 0.602.

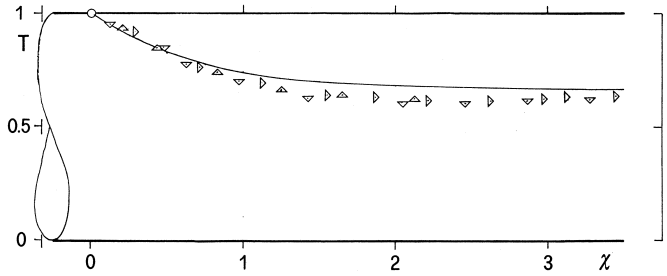

Fig. 10. Cavity profile $T(\chi)$ for f = (Δ) 0.641; (▽) 0.628, (▷) 0.602 and (—) (15).

Note the discontinuity in slope at the upper outflow crest, where the velocity is equal to zero [Fig. 9(a)]. For $f = 0.794$ and 0.700, reference is made to bubble washout, and the end depth ratio is significantly reduced, with the bubble length of the order of D [Fig. 9(b) and (c)]. Typical cavity flow occurs for $f = 0.641$ and 0.628 [Fig. 9(d) and (e)] and the horizontal flow portion is now developed. For $f = 0.602$, the cavity length is $7D$, with a single small wave [Fig. 9(f)]. The flow was so stable that the wave remained small, and wave breaking never occurred.

The surface profile $T(\chi)$ for cavity outflow is shown in Fig. 10, together with the prediction (15). The computed asymptotic flow depth is somewhat too large, and an average experimental value is $T = 0.63$ instead of (2/3). The bubble slope close to the stagnation point is practically constant $dT/d\chi = -0.5$, independent of the exact value of f. The corresponding downstream Froude number is $\mathbf{F} = Q/(gDh^4)^{1/2} = (\pi/4y^2)f \cong 1.23$ when assuming $f = 0.62$ as an average value. For such **F**, undular surface waves of small wave height are typical.

The end depth ratio $y_e = h_e/D$ varies with f as predicted in (17). Fig. 11(a) shows substantial agreement between the momentum approach and the data. The effect of bottom slope ($-1\% \leqslant S_0 \leqslant +1\%$) is small, except close to the transition for free surface flow ($f < 0.6$), as previously discussed. The data could also be approximated with

$$y_e = \frac{5}{6}f, \quad 0.5 \leq y_e \leq 1. \tag{18}$$

For a given pipe diameter, the end depth thus increases linearly with the full pipe velocity V.

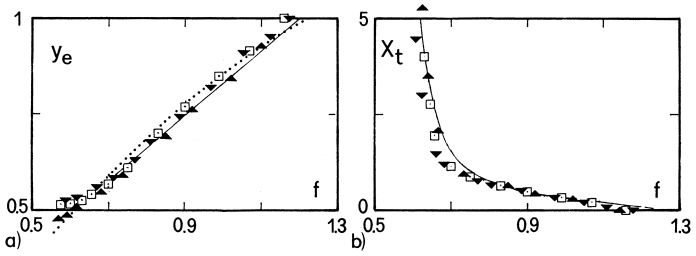

Fig. 11. (a) End depth ratio $y_e(f)$ for S_0 = (▼) −1%, (□) 0, (▲) +1% and (...) (17), (—) (18); (b) relative distance of stagnation point $X_t(f)$ (—) (19).

The distance of the stagnation point from the end section $X_t = x_t/D$ is shown in Fig. 11(b), as a function of f. With the fictitious transition pipe Froude number $f_t = 0.55$, the data follow

$$X_t = 0.09(f - f_t)^{-3/2},\ 0.6 < f < 1.2. \tag{19}$$

For cavity washout, the distance decreases almost linearly with f as $[X_t - (4/3)]/(f - f_t) = -2$, whereas the decrease for cavity outflow is larger with increasing f, as given with (19).

8. Nappe trajectories

The lower and upper nappes of free surface flow in a circular pipe were investigated by Clausnitzer and Hager (1997). For an approach flow depth $h_0 < D$ and an approach Froude number $\mathbf{F}_0 = Q/(gDh_0^4)^{1/2}$, the end depth ratio $Y_e = h_e/h_0$ is

$$Y_e = \left(\frac{2\mathbf{F}_0^2}{1 + 2\mathbf{F}_0^2}\right)^{2/3}. \tag{20}$$

The lower nappe trajectory $z_t(x_t)$ with the origin at the bottom of the end section and z_t measured positively downwards [Fig. 8(b)] depended essentially on the streamwise coordinate $X_0 = (x_t/h_0)\mathbf{F}_0^{-0.8}$. For the present configuration, the lengths were related to the end depth h_e instead of the upstream approach depth h_0. Fig. 12(a) shows that $Z_e = z_t/h_e$ can be related to $X_e = (x_t/h_e)\mathbf{F}_e^{-0.8}$ with the scaling Froude number $\mathbf{F}_e = Q/(gDh_e^4)^{1/2}$ as

$$Z_e = \frac{1}{3}X_e + \frac{1}{4}X_e^2,\ f \le 0.79. \tag{21}$$

The previous relation established by Clausnitzer and Hager applies thus also for $Z_e(X_e)$, instead of $Z_0(X_0)$. For $f > 0.79$, some deviation is caused by the modified outflow configuration.

The axial nappe thickness $Z_t(X_e)$ with $Z_t = t_t/h_e$ is shown in Fig. 8(b). Whereas the nappe thickness increases for free surface outflow when normalized with h_0 (Clausnitzer and Hager,

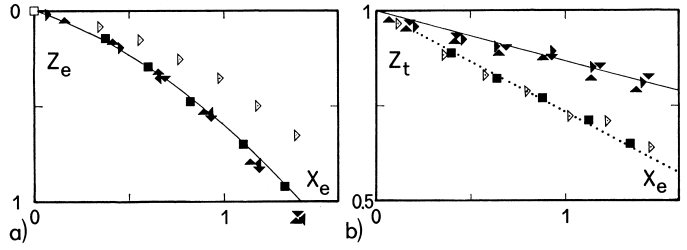

Fig. 12. Nappe trajectories for cavity outflow (a) lower nappe $Z_e(X_e)$ with (—) (21); (b) axial nappe thickness $Z_t(X_e)$ with (—) (22). f = (▼) 0.628, (▶) 0.641, (▲) 0.700, (■) 0.794, (▷) 1.19.

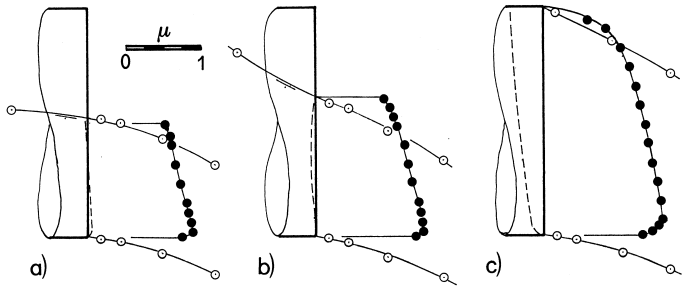

Fig. 13. Axial velocity distribution at end section $\mu(Z)$ for f = (a) 0.628; (b) 0.75; (c) 1.16. (●) Local velocity, (○) trajectory geometry, (- - -) pressure distribution for potential flow.

1997), the nappe thickness decreases in the present case as [Fig. 12(b)]

$$Z_t = 1 - 0.265\nu X_e \tag{22}$$

where $\nu = 1$ for $f \leqslant 0.70$ (cavity outflow), and $\nu = 2$ for $f > 0.70$ (bubble washout).

9. Velocity distribution

Fig. 13 shows dimensionless axial velocity distributions $\mu(Z)$ where $\mu = v/(gD)^{1/2}$ and $Z = z/D$. In all cases, the velocity increases from the upper to the lower trajectory. For $f = 0.628$ the velocity increase is almost linear, and the pressure head based on the assumption of constant energy is practically zero [Fig. 13(a)]. For $f = 0.75$ (bubble washout) the velocity distribution is similar to Fig. 13(a) but there is a slight negative pressure at the end section [Fig. 13(b)]. For $f = 1.16$, finally, i.e. the transition from bubble washout to pressurized pipe flow, the velocity is practically equal to zero at the pipe vertex, associated with a significant subpressure of almost $-0.5(\rho gD)$, and the velocity increases significantly at the lower trajectory associated with a decrease of internal pressure [Fig. 13(c)]. The negative pressure force is $-0.304\ (\rho g\pi D^2/4)$, with the average velocity $1.17(gD)^{1/2}$.

10. Conclusions

Cavity outflow from a nearly horizontal pipe is investigated, based on detailed experimentation and a hydraulic approach. The agreement between predictions and observations is satisfactory, and the pipe Froude number f is the main variable.

Based on a literature review, one should rather refer to the Cola bubble than the Benjamin bubble. A bubble may be fixed with a corresponding approach discharge and observations can be conducted for steady rather than for unsteady flow conditions. The cavity shape is described in terms of f, and bubble washout is distinguished from cavity outflow. The shape of the cavity profile is determined, based on an extended Boussinesq equation. Eq. (15) is in agreement with observations for cavity outflow. The end depth ratio, and the location of the stagnation point

relative to the end section are determined. Finally, the lower nappe profile and the nappe thickness are specified, based on an earlier approach for free surface pipe outflow.

References

Alves, I.N., Shoham, O., Taitel, Y., 1993. Drift velocity of elongated bubbles in inclined pipes. Int. J. Multiphase Flow 48 (17), 3063–3070.

Baines, W.D., Rottmann, J.W., Simpson, J.E., 1985. The motion of constant-volume air cavities in long horizontal tubes. J. Fluid Mech. 161, 313–327.

Bendiksen, K.H., 1984. An experimental investigation of the motion of long bubbles in inclined tubes. Int. J. Multiphase Flow 10 (4), 467–483.

Benjamin, T.B., 1968. Gravity currents and related phenomena. J. Fluid Mech. 31, 209–248.

Clausnitzer, B., Hager, W.H., 1997. Outflow characteristics from circular pipe. J. Hydraul. Engng. 123 (10), 914–917.

Cola, R., 1965. Onde di vuotamento di un ambiente a pressione. L'Energia Elettrica 42 (3), 163–174.

Cola, R., 1967. Esame teorico e sperimantale dei fenomeno ondosi di vuotamento di una condotta a sezione circolare. Atti dell'Istituto Veneto di Scienze, Lettere ed Arti 125, 257–294.

Cola, R., 1970. Sul moto permanente in prossimità del sbocco di una condotta a sezione circolare. L'Acqua 48 (3), 70–79.

Couët, B., Strumolo, G.S., 1987. The effects of surface tension and tube inclination on a two-dimensional rising bubble. J. Fluid Mech. 184, 1–14.

Hager, W.H., 1983. Hydraulics of plane free overflow. J. Hydraul. Engng. 109 (12), 1683–1697.

Hager, W.H., Hutter, K., 1984. Approximate treatment of plane channel flow. Acta Mech. 51, 31–48.

Liggett, J.A., 1994. Fluid Mechanics. McGraw-Hill, New York.

Montes, J.S., 1997. Transition to a free-surface flow at the end of a horizontal conduit. J. Hydraul. Res. 35 (2), 225–241.

Wallis, G.B., Crowly, C.J., Hagi, Y., 1977. Conditions for a pipe to run full when discharging liquid into a space filled with gas. J. Fluids Engng. 99 (6), 405–413, 100 (3), 136.

Wilkinson, D.L., 1982. Motion of air cavities in long horizontal ducts. J. Fluid Mech. 118, 109–122.